Force-sensing LPHN2 is indispensable for normal hearing and mediates MET in cochleae through Gs and CNGA3 coupling

Zhao Yang[1,3#], Ming-Wei Wang[4#], Shu-Hua Zhou[1,2#], Zhi-Chen Song[2#], Jia-Rui Gao[2#], Wen-Wen Liu[8], Qi-Yue Zhang[1], Ying Guan[1,3], Lei Xu[8], Chuan Wang[7*], Zhi-Gang Xu[6*], Xiao Yu[2*], Jin-Peng Sun[1,3,4,5*]

Affiliations:

[1]NHC Key Laboratory of Otorhinolaryngology, Qilu Hospital of Shandong University, and Department of Biochemistry and Molecular Biology, School of Basic Medical Sciences, Cheeloo College of Medicine, Shandong University, Jinan 250012, China.

[2]Key Laboratory of Experimental Teratology of the Ministry of Education, Department of Physiology, School of Basic Medical Sciences, Cheeloo College of Medicine, Shandong University, Jinan 250012, China.

[3]Advanced Medical Research Institute, Cheeloo College of Medicine, Shandong University, Jinan 250012, China.

[4]Department of Clinical Laboratory, The Second Hospital, Cheeloo College of Medicine, Shandong University, Jinan 250012, China.

[5]Key Laboratory of Molecular Cardiovascular Science of the Ministry of Education, Department of Physiology and Pathophysiology, School of Basic Medical Sciences, Peking University, Beijing 100191, China.

[6]Shandong Provincial Key Laboratory of Animal Cells and Developmental Biology, Shandong University School of Life Sciences, Qingdao 266237, China

[7]Department of Pharmacology, Hebei Medical University, Shijiazhuang 050000, China

[8]Department of Otolaryngology-Head and Neck Surgery, Shandong Provincial ENT Hospital, Cheeloo College of Medicine, Shandong University, Jinan 250014, China.

# These authors contributed equally to this work.

* Correspondence: Jin-Peng Sun, E-mail: sunjinpeng@sdu.edu.cn

Xiao Yu, E-mail: yuxiao@sdu.edu.cn

Zhi-Gang Xu, E-mail: xuzg@sdu.edu.cn

Chuan Wang, E-mail: wangchuan@hebmu.edu.cn

Abstract

Auditory perception enables acoustic experiences, including listening to melodious music and engaging in linguistic communication. Conversion of the force sensation into electrical signals via mechanoelectrical transduction (MET) in cochlear hair cells is the key step for auditory perception; however, the sound receptor for auditory perception at the molecular level is not clear. Here, we found that hair cell-specific deficiency of the G protein-coupled receptor LPHN2 in *Pou4f3-CreER*$^{+/-}$*Lphn2*$^{fl/fl}$ mice or pharmacological blockade of CNG ion channels in mice severely impaired hearing. Importantly, sensation of force by LPHN2 not only increased intracellular cAMP and calcium levels but also elicited rapid membrane depolarization of cochlear hair cells via Gs-dependent CNGA3 coupling. Both LPHN2 and CNGA3 were expressed at the stereocilia and cuticular plates and associated with each other. Notably, hearing loss in LPHN2-deficient mice was almost fully reversed by re-expression of LPHN2-GAIN in cochlear hair cells. Therefore, we propose that LPHN2 acts as a direct sound sensor in cochlear hair cells by mediating MET through Gs and CNGA3 coupling. Furthermore, both GPCR members and ion channels modulated by second messengers might actively participate in the MET process during auditory perception.

Introduction

Auditory perception is one of our basic senses and provides us with the opportunity to experience the features of an acoustic world, including melodious music, the chirps of birds and the tinkling of spring water. It is also our main gateway for communicating with each other via speech and alerts us to possible dangers. By converting mechanical force into electrical signals, mechanoelectrical transduction (MET) in cochlear hair cells acts as the central event during auditory perception (Zheng and Holt, 2021). Importantly, recent studies have identified a series of candidate components of the MET channel complex, which include the transmembrane membrane proteins TMC1/2, TMIE, and LHFPL5 and auxiliary subunits such as calcium (Ca^{2+}) and integrin binding protein 2 (CIB2) and ankyrin (Cunningham et al.,

2020; Liang et al., 2021; Pan et al., 2013; Tang et al., 2020; Xiong et al., 2012). Despite several findings suggesting that TMC1 and TMC2 are probable pore-forming subunits of the MET channel complex, direct evidence for force sensation by TMC1/2 is lacking (Jia et al., 2020; Pan et al., 2018). In addition to these MET components concentrated at the tips of the stereocilia, another mechanosensitive ion channel, Piezo2, which is expressed at the cuticular plates of cochlear hair cells, has also been suggested to be a MET regulator (Wu et al., 2017). Despite the significant progress in research, the molecular mechanisms underlying MET in cochlear hair cells are unclear, and the components of MET have not been fully elucidated.

In addition to ion channels, G protein-coupled receptors (GPCRs) are well known to function as important sensory receptors that mediate the sensation of light, odour, itch and at least three qualities of taste (Buck and Axel, 1991; Yang et al., 2021; Yau and Hardie, 2009; Zhang et al., 2003). Importantly, several GPCRs expressed in the cochlea have been shown to be essential for hearing. For instance, whereas CELSR1 and Fzd3/6 are required for the maintenance of cochlear planar cell polarity, LGR5 regulates the self-renewal abilities of cochlear hair cells (Duncan et al., 2017; Shi et al., 2013; Wang et al., 2006). Moreover, many mutations of VLGR1 are responsible for severe hearing loss (Guan et al., 2023). Although GPCRs play important regulatory roles in cochlear development, it is still unknown whether GPCRs directly participate in the MET process and regulate auditory perception.

In our parallel work described in two companion papers, we found that two adhesion GPCRs, GPR133 and LPHN2, act as equilibrioceptors by directly sensing force and mediating MET in vestibular hair cells. In our present study, we further found that mechanosensitive LPHN2 showed a unique distribution in cochlear hair cells, being immunostained at both stereocilia and cuticular plates. Global knockout or hair-cell-specific knockout of *Lphn2* in mice impaired hearing. Mechanistically, force sensation by LPHN2 induced rapid Ca^{2+} signalling and acute membrane current changes by activating the Gs-cAMP-CNGA3 signalling axis. Furthermore, pharmacological inhibition of CNGA3 activity abrogated LPHN2-mediated MET and caused hearing impairment in mice. Overall, our findings identify a mechanosensitive GPCR that directly participates in the effects of MET on hearing through functional coupling to CNGA3.

Results

Expression of LPHN2 in cochlear hair cells

Previous single-cell RNA sequencing (scRNA-seq) data have indicated that LPHN2 is expressed primarily in cochlear hair cells with a dynamic pattern (Ranum et al., 2019). The LPHN2 expression frequency decreased from approximately 75% in embryonic cochlear hair cells to ~ 42% after birth (Figure S1A). Consistently, the mRNA level of *Lphn2* in the mouse cochlear epithelium showed an approximately 30% decline from E20 to P14 and then reached a steady-state level at P30 (Figure 1A). The protein level of LPHN2 in cochlear hair cells was approximately 387 fmol/mg as measured by western blotting (using the purified LPHN2 proteins as the reference), which is approximately 1.5-fold higher than that of VLGR1 at P10 (Figure S1B-1C).

Importantly, via separation of the stereocilia from the hair cell body using the twist-off method (Avenarius et al., 2017), we were able to detect the expression of LPHN2 in both stereocilia and cell bodies of cochlear hair cells using PCDH15 and Myosin7a as specific markers for stereocilia and the hair cell body, respectively (Figure 1B and Figure S1D-1E). In contrast, LPHN2 was detected only at the cell body but not in the stereocilia of utricular hair cells, which was consistent with the immunostaining results in our parallel study (Figure 1B and Figure S1D-1E). To further explore the expression pattern of LPHN2 in mouse cochlear hair cells, we employed whole-mount immunostaining using a commercial LPHN2 antibody, which showed specificity in both HEK293 cells overexpressing LPHN2 or cochleae derived from *Lphn2*$^{-/-}$ mice at E18 (Figure S1F-1G). Different optical sections from the stereocilia to the cochlear hair cell body were examined to monitor the subcellular localization of LPHN2 (Figure 1C). Notably, in cochlear outer hair cells (OHCs) of mice at P30, LPHN2 immunofluorescence puncta were observed along the length of stereocilia, with staining at the tips of several stereocilia (Figure 1D and Figure S1H). LPHN2 immunofluorescence was also observed at the apical surfaces of OHCs, which was further supported by coimmunostaining of LPHN2 with Spectrin, a specific marker of the cuticular plate, and by staining of sections of the cochlear sensory epithelium using Myosin7a as the hair cell marker (Figure 1E-1F). In contrast, LPHN2 expression was not detected at the basolateral membrane along the cell bodies of OHCs (Figure 1F). A similar expression pattern of LPHN2 was also observed in

cochlear inner hair cells (IHCs), showing a distribution along the stereocilia and at the cuticular plate (Figure 1D-1F and Figure S1H). The specific expression pattern of mechanosensitive LPHN2 in cochlear hair cells, especially its localization at the stereocilia, suggests that LPHN2 might have unique functions in the vestibular systems.

LPHN2 deficiency severely impairs hearing

To inspect the functional roles of LPHN2 in hearing, we initially employed heterozygous *Lphn2* gene knockout (*Lphn2*$^{+/-}$) mice since *Lphn2*$^{-/-}$ mice show embryonic lethality (Anderson et al., 2017) (Figure S2A-2C). The *Lphn2*$^{+/-}$ mice were viable and showed normal growth but displayed vestibular defects in our parallel study. Measurement of the auditory brainstem response (ABR) revealed that *Lphn2*$^{+/-}$ mice at P30 had an approximately 2-fold (~30 dB) higher auditory threshold than their wild-type (WT) littermates in response to click stimuli (Figure 2A). Moreover, compared with the WT mice, the *Lphn2*$^{+/-}$ mice showed significantly elevated ABR thresholds at different frequencies (4, 8, 12, 16, 24 and 32 kHz) (Figure 2A-2B). Analysis of ABR wave I tests further indicated a lower wave amplitude and increased wave latency of *Lphn2*$^{+/-}$ mice, suggesting that the function of IHCs in *Lphn2*$^{+/-}$ mice was impaired (Figure 2C). Furthermore, the distortion-product otoacoustic emission (DPOAE) in *Lphn2*$^{+/-}$ mice was significantly elevated between 12 and 24 kHz, implying that OHC function was affected in *Lphn2*$^{+/-}$ mice (Figure 2D). Since the deterioration of hearing functions might have been due to developmental defects of hair cells, we examined the morphology of hair cells by immunostaining and scanning electron microscopy. Importantly, the results from both analyses revealed no detectable impairment in the structure or morphology of OHCs and IHCs in the cochleae of *Lphn2*$^{+/-}$ mice, suggesting that the heterozygous ablation of LPHN2 in mice did not, at least at the age of 4 weeks, cause developmental defects of cochlear hair cells (Figure S2D-2F).

To further assess the specific role of LPHN2 in cochlear hair cells, we crossed *Lphn2*$^{fl/fl}$ mice with an inducible *Pou4f3-CreER*$^{+/-}$ transgenic mouse line (Figure S2G). Previous scRNA-seq data (GSE114157) have indicated that POU4F3, which is a commonly used hair cell marker, is expressed in all LPHN2-positive cochlear hair cells; therefore, we deemed that the use of *Pou4f3-CreER*$^{+/-}$*Lphn2*$^{fl/fl}$ mice should enable hair cell-specific ablation of LPHN2.

Consistently, specific ablation of LPHN2 in the cochleae and utricles of *Pou4f3-CreER*$^{+/-}$ *Lphn2*$^{fl/fl}$ mice was indicated by both immunofluorescent and western blotting (Figure S2H-2J). In contrast, LPHN2 expression in other tissues of *Pou4f3-CreER*$^{+/-}$*Lphn2*$^{fl/fl}$ mice, such as the brain, was not significantly affected (Figure S2H-2I). Notably, compared with their control *Pou4f3-CreER*$^{+/-}$*Lphn2*$^{+/+}$ littermates, the *Pou4f3-CreER*$^{+/-}$*Lphn2*$^{fl/fl}$ mice displayed severely impaired hearing in terms of the elevated ABR threshold at all testing frequencies and deteriorated DPOAE between 8 and 32 kHz (Figure 2E-2H). Consistent with the observation in *Lphn2*$^{+/-}$ mice, the *Pou4f3-CreER*$^{+/-}$*Lphn2*$^{fl/fl}$ mice at P30 also showed normal structure and morphology of cochlear hair cells (Figure 2I-2J and Figure S2K). Collectively, these findings support the idea that LPHN2 expressed in cochlear hair cells is essential for hearing and suggest that LPHN2 regulates hearing functions potentially through an instantaneous physiological process.

Force sensation by LPHN2 results in increased cAMP and rapid Ca^{2+} signals

GPCRs act as direct sensors of itch or in the senses of vision, smell, and taste by converting extracellular stimuli into alterations in the intracellular levels of second messengers, such as cAMP, cGMP and Ca^{2+} (Filipek et al., 2003; Guo et al., 2023; Kaupp, 2010; Smith, 2023; Yang et al., 2021; Yang et al., 2023). Our parallel study indicated that LPHN2 activates Gs and Gi signalling in response to force stimulation (Figure S3A-3B). We therefore measured cAMP levels after delivering force to LPHN2 in cochlear explants using paramagnetic beads coated with an anti-LPHN2 antibody (referred to as LPHN2-M-beads) that recognize the N-terminus (residues 551-600) of LPHN2 and can exert quantifiable force on LPHN2 in a magnetic field. Importantly, application of 3 pN of force on the cochlear sensory epithelium derived from *Pou4f3-CreER*$^{+/-}$*Lphn2*$^{+/+}$ mice induced an approximately 1.6-2.2-fold increase in the intracellular cAMP levels at different sections (apex turn: from 1.49 ± 0.11 mM to 2.41 ± 0.13 mM; middle turn: from 1.58 ± 0.07 mM to 3.41 ± 0.18 mM; base turn: from 1.51 ± 0.08 mM to 2.48 ± 0.14 mM), which was abrogated in the cochlear explants pretreated with the Gs-specific inhibitor NF449 or in cochlear explants from *Pou4f3-CreER*$^{+/-}$*Lphn2*$^{fl/fl}$ mice at P10 (Figure 3A). In contrast, the force applied by paramagnetic beads coated with polylysine (referred to as Ctrl-beads) did not induce detectable cAMP responses in the cochlear explants

(Figure S3C). These results suggest that the Gs-cAMP pathway downstream of LPHN2 is activated in response to force stimulation in the cochlea. Consistent with these findings, the Gs protein was found to be the most abundantly expressed among all the G protein subtypes in LPHN2-expressing cochlear hair cells, as revealed by both scRNA-seq data and the single-cell qRT-PCR analysis of 20 isolated cochlear hair cells (Figure 3B and Figure S3D).

The mechanical stimulation-triggered Ca^{2+} signal in cochlear hair cells was hypothesized to regulate the rate of neurotransmitter release, which is essential for the transmission of sound information. To record the force-induced Ca^{2+} response at the single-cell level, we treated P3 mice with a modified AAV-ie-*Lphn2pr*-mCherry, which enabled specific fluorescent labelling of the LPHN2-expressing hair cells, through round window membrane injection. The cochleae were isolated at P10, and mCherry-labelled hair cells were selected for Ca^{2+} imaging using a Fura-2 fluorescent probe. Notably, approximately 25% (15 out of 60) of the LPHN2-expressing cochlear hair cells showed a rapid Ca^{2+} response to LPHN2-M-bead-mediated force stimulation, which was recorded within 140 to approximately 340 ms after force application (Figure 3C-3E and Figure S3E-3F). In contrast, none of the unlabelled hair cells or the mCherry-labelled hair cells derived from *Pou4f3-CreER*$^{+/-}$*Lphn2*$^{fl/fl}$ mice showed detectable Ca^{2+} signals in response to force application, suggesting the specificity of the mechanical force-mediated Ca^{2+} response through activation of LPHN2 (Figure 3C-3E and Figure S3E-3F). The force-stimulated Ca^{2+} response in LPHN2-expressing cochlear hair cells was concentration-dependently inhibited by pretreatment with the Gs inhibitor NF-449 with an EC50 of 412 ± 19 nM, which was similar to the inhibitory EC50 of NF-449 (272 ± 44 nM) in a heterologous system towards force-stimulated LPHN2-Gs-cAMP signalling (Figure 3F-3G and Figure S3G-3K). In contrast, the force-stimulated Ca^{2+} response was not affected by pretreatment with the Gq inhibitor YM-254890 (Figure 3F and Figure S3H). Moreover, the force application via LPHN2-M-beads showed no detectable effects on the intracellular levels of IP3, the critical downstream messenger of the Gq pathway (Figure S3L). These results suggested that force-stimulated activation of LPHN2 in cochlear hair cells induces rapid Ca^{2+} signals in a Gs-dependent and Gq-independent manner, potentially due to extracellular Ca^{2+} influx rather than mobilization from the intracellular Ca^{2+} store of IP3R. Consistent with this hypothesis, incubation of the cochlear explants in a Ca^{2+}-deficient bath completely abolished

the force-induced Ca^{2+} response in LPHN2-expressing hair cells (Figure 3F and Figure S3I). We therefore speculate that an ion channel activated by Gs signalling may contribute to extracellular Ca^{2+} influx in response to LPHN2 activation after force engagement in cochlear hair cells.

Force sensation by LPHN2 elicits acute currents in cochlear hair cells

The opening of Ca^{2+}-permeable MET channels at the stereocilia bundles of hair cells is a key step in auditory transduction, which induces inward current and depolarizes the hair cell membrane (Douguet and Honore, 2019; Jeong et al., 2022; Jung and Muller, 2023; Wu et al., 2017; Zheng and Holt, 2021). The force-induced rapid Ca^{2+} influx in cochlear hair cells through activation of LPHN2 suggests the potential participation of LPHN2 in the MET process. We therefore examined the excitability of cochlear hair cells in response to force stimulation of LPHN2. The whole-cell patch-clamp recording revealed that approximately 23% (15 out of 65, cluster I) of AAV-i.e.-*Lphn2pr*-mCherry-labelled cochlear hair cells derived from *Pou4f3-CreER*$^{+/-}$*Lphn2*$^{+/+}$ mice showed an approximately 50% increase in current amplitude in response to 3 pN force stimulation applied by LPHN2-M-beads, whereas the other 77% (50 out of 65, cluster II) showed no detectable changes (Figure 4A-4B and Figure S4A-4B). In contrast, the AAV-ie-*Lphn2pr*-mCherry-labelled hair cells in the cochlear explants derived from *Pou4f3-CreER*$^{+/-}$*Lphn2*$^{fl/fl}$ mice showed no significant electrophysiological responses to force stimulation with LPHN2-M-beads (Figure 4A-4B and Figure S4A). Nevertheless, similar to those of their WT counterparts, the cochlear hair cells of *Pou4f3-CreER*$^{+/-}$*Lphn2*$^{fl/fl}$ mice could also be divided into cluster I cells (10 out of 40, 25%) and cluster II cells (30 out of 40, 75%) according to their electrophysiological characteristics (Figure 4A-4B). In particular, the cluster I cochlear cells derived from either *Pou4f3-CreER*$^{+/-}$ *Lphn2*$^{+/+}$ or *Pou4f3-CreER*$^{+/-}$*Lphn2*$^{fl/fl}$ mice featured outwardly rectifying voltage-dependent currents, showing a higher maximum amplitude than the cluster II cells at the same holding potential (Figure 4A-4B).

To further analyse the excitability of cochlear hair cells downstream of LPHN2 in response to force sensation, we recorded the resting membrane potential of cluster I cells using a current clamp. Notably, when holding at 0 pA, 3 pN force stimulation with LPHN2-M-beads

induced a significant depolarization of the WT cluster I cells by elevating the resting membrane potential from -80 mV to approximately -65 mV (Figure 4C). As the negative controls, the cluster I hair cells showed no significant alteration of membrane potential in response to force stimulation with Ctrl-beads (Figure 4C).

Notably, the kinetic analysis of the force-induced membrane potential alteration revealed that the activation time, which was defined as the time between the force application and the rise of the membrane potential, was 94.6 ± 16.4 ms (Figure 4C-4D). In addition, after force removal, the hair cell membrane potential quickly returned to the basal level with a delay time of 97.0 ± 15.0 ms and a recovery time constant (τ_{rec}) of 110.4 ± 18.5 ms (Figure 4C-4D). The very rapid activation time indicates the presence of an acute current in cochlear hair cells in response to force stimulation applied by LPHN2-M-beads, which is consistent with the force-induced rapid Ca^{2+} response in LPHN2-expressing hair cells. Similar to the dependency of the rapid Ca^{2+} response on the LPHN2-Gs pathway, the LPHN2-M-bead-mediated current change was also dose-dependently inhibited by pretreatment with the Gs inhibitor NF449, with an inhibitory EC50 of 515 ± 84 μM (Figure 4E and Figure S4C-4D). Moreover, the force-stimulated membrane potential alteration of cochlear hair cells was also abrogated by treatment with NF449 (Figure 4F). Notably, the LPHN2-mediated current response was much faster than that obtained for the LPHN2-expressing utricular hair cells in our parallel study (94.6 ± 16.4 ms vs. 704.7 ± 9.0 ms), suggesting that LPHN2 might be part of the MET machinery in the cochlear hair cells that directly participates in auditory perception (Figure 4G). Consistently, FM1-43 uptake by *Pou4f3-CreER*$^{+/-}$*Lphn2*$^{+/+}$ cochlear hair cells, which is commonly utilized to evaluate MET channel activity, was significantly increased in response to force stimulation with LPHN2-M beads within 5 seconds (Figure 4H and Figure S4E). Notably, the force-induced stimulatory effect on FM1-43 uptake was abolished in *Pou4f3-CreER*$^{+/-}$*Lphn2*$^{fl/fl}$ cochlear hair cells or by pretreatment with 10 μM NF449 in *Pou4f3-CreER*$^{+/-}$*Lphn2*$^{+/+}$ cochlear explants (Figure 4H and Figure S4E). Collectively, these results support the idea that force-stimulated LPHN2 activation in cochlear hair cells promotes membrane depolarization by eliciting acute currents in a Gs-dependent manner (Figure 4G).

Functional coupling of mechanosensitive LPHN2 to CNGA3 in cochlear hair cells

The increased intracellular cAMP levels and the Gs-dependent rapid Ca^{2+} response and membrane excitation downstream of the mechanosensitive LPHN2 in cochlear hair cells recall the signalling mechanism for olfactory perception, which involves cyclic nucleotide-gated (CNG) cation channels. Suspecting that a similar mechanism might exist in cochlear hair cells, we examined the expression patterns of CNG channels and another family of cyclic nucleotide-regulated cation channels, hyperpolarization-activated cyclic nucleotide–modulated (HCN) channels, in LPHN2-expressing cochlear hair cells by analysing scRNA-seq data (GSE114157). We found that 4 out of 6 CNG channels (CNGA1, CNGA2, CNGA3 and CNGB1) and all 4 HCN channels were expressed in LPHN2-positive cochlear hair cells (Figure S5A). Notably, 5 of these channels, including CNGA3, CNGB1 and HCN1-3, showed a high expression frequency (37~58%) in LPHN2-expressing hair cells (Figure S5A). Further qRT□PCR analysis of single LPHN2-expressing hair cells revealed that CNGA3 was specifically expressed in cluster I hair cells (Figure 5A). HCN1 also showed elevated expression in cluster I hair cells, whereas the other channels were similarly expressed in cluster I and II cells (Figure 5A). Consistent with our findings in the utricular hair cells in the parallel study, the LPHN2 precipitated from the cochlear hair cells by LPHN2-M-beads showed specific interaction with CNGA3 but not the other channel proteins (Figure 5B and Figure S5B). Moreover, LPHN2 coimmunostained with CNGA3 both at the stereocilia and the cuticular plates of the cochlear hair cells derived from mice at P30, suggesting the occurrence of a direct interaction between LPHN2 and CNGA3 in vivo (Figure 5C).

To explore the potential roles of CNGA3 in hearing, we exploited the CNG inhibitor L-cis-diltiazem and examined its effects on the auditory function of mice. Notably, intraperitoneal injection of L-cis-diltiazem for 3 consecutive days significantly elevated the ABR threshold at click and different testing frequencies of mice, which resembled the hearing performance of *Lphn2*-deficient mice (Figure S5C-5E). Moreover, L-cis-diltiazem administration induced deteriorated DPOAE compared with that of the mice treated with the control vehicle, resulting in elevated thresholds at testing frequencies between 12 and 24 kHz (Figure S5F). To inspect the specific role of CNGA3 in cochlear hair cells, we generated a *Pou4f3-CreER*$^{+/-}$ *Cnga3*$^{fl/fl}$ mouse line in which *Cnga3* was specifically ablated in hair cells in an inducible manner. Compared with their *Pou4f3-CreER*$^{+/-}$*Cnga3*$^{+/+}$ littermates, the heterozygous *Pou4f3-*

CreER$^{+/-}$*Cnga3*$^{fl/+}$ mice showed significantly impaired auditory performance, including elevated ABR thresholds at all testing frequencies, increased latency and reduced amplitudes of ABR wave I, and deteriorated DPOAE between 12 and 24 kHz (Figure 5D-5E and Figure S5G-5H). These results indicated a critical role of the CNGA3 channel in normal hearing.

To further investigate whether CNGA3 directly participates in the mechanosensitive LPHN2-mediated rapid auditory response, we examined the effects of L-cis-diltiazem application on the Ca^{2+} response and acute current in LPHN2-expressing hair cells in response to force applied by LPHN2-M-beads. Our results indicated that both the force-stimulated rapid Ca^{2+} response and acute currents were significantly diminished in cochlear hair cells pretreated with L-cis-diltiazem in a dose-dependent manner, with EC50 values of 36 ± 2 μM and 31 ± 5 μM, respectively (Figure 5F-5I and Figure S5I-5J). Moreover, administration of 100 μM L-cis-diltiazem abolished the force-stimulated membrane potential alteration of cochlear hair cells and decreased the force-stimulated FM1-43 uptake in the cochlear hair cells by approximately 80% (Figure 5J-5K and Figure S5K). To investigate the potential nonspecificity of L-cis-diltiazem by inhibiting other ion channels, we examined the inhibitory potency of L-cis-diltiazem on different CNG or HCN channels in the heterologous system. The inhibitory EC50 of L-cis-diltiazem on CNGA3 in HEK293 cells was 38 ± 5 μM, which was similar to that recorded for L-cis-diltiazem on the force-induced current changes in the cochlear explants (31 ± 5 μM) (Figure S6A-6B). In contrast, L-cis-diltiazem showed significantly lower potency in inhibiting CNGA1 in the heterologous system (EC50: 70 ± 10 μM), and it did not affect the HCN activities even at the high concentration of 500 μM (Figure S6C-6H). Therefore, these results support the hypothesis that L-cis-diltiazem regulates the mechanosensitive LPHN2-mediated effects primarily by inhibiting the CNGA3 channel in vivo. In addition, our parallel study indicated that force application to LPHN2 in heterologous HEK293 recombination systems was able to activate CNGA3 channels in vitro (Figure S6I-6J). Collectively, these results suggest the existence of a functional coupling between mechanosensitive LPHN2 and CNGA3 in cochlear hair cells that regulates the LPHN2-mediated rapid response and potentially contributes to auditory perception.

LPHN2 re-expression in cochlear hair cells of Lphn2-deficient mice reverses hearing loss

To further explore the functional roles of LPHN2 in the peripheral auditory system, especially in cochlear hair cells, we next performed an in vivo rescue experiment by delivering LPHN2-encoding AAV-ie into the cochleae of *Pou4f3-CreER*$^{+/-}$*Lphn2*$^{fl/fl}$ mice and examined its effects on the auditory functions of these *Lphn2*-deficient mice. The LPHN2-GAIN construct with the deletion of 523 N-terminal residues, which showed mechanosensitive potential compared to that of full-length LPHN2, was packed into the AAV-ie-*Lphn2pr*-mCherry vector (referred to as AAV-ie-LPHN2) and delivered into P3 *Pou4f3-CreER*$^{+/-}$*Lphn2*$^{fl/fl}$ mice through round window membrane injection (Figure S7A). The specific expression of LPHN2-GAIN in the cochleae and utricles, but not the brains, of *Pou4f3-CreER*$^{+/-}$*Lphn2*$^{fl/fl}$ mice was observed using western blotting after the administration of AAV-ie-LPHN2 (Figure S7B). In particular, LPHN2 was re-expressed at the stereocilia and cuticular plates of both cochlear OHCs and IHCs of AAV-ie-LPHN2-treated *Pou4f3-CreER*$^{+/-}$ *Lphn2*$^{fl/fl}$ mice (Figure S7C). In contrast, no LPHN2-GAIN expression was detected in the cochleae of *Pou4f3-CreER*$^{+/-}$*Lphn2*$^{fl/fl}$ mice treated with the control virus AAV-ie-*Lphn2pr*-mCherry (Figure S7C).

We next assessed the auditory functions of mice receiving LPHN2-GAIN gene delivery. Notably, the *Lphn2*-deficient mice treated with AAV-ie-LPHN2 showed significantly improved performance in the ABR test. The ABR thresholds at all testing frequencies, as well as the amplitude and latency of ABR wave I, of AAV-ie-LPHN2-treated *Pou4f3-CreER*$^{+/-}$ *Lphn2*$^{fl/fl}$ mice returned to levels comparable to those of *Pou4f3-CreER*$^{+/-}$*Lphn2*$^{+/+}$ mice (Figure 6A-6C and Figure S7D). Moreover, the DPOAE thresholds of the *Lphn2*-deficient mice were also restored to nearly normal levels after AAV-ie-LPHN2 treatment (Figure 6D). As negative controls, *Lphn2*-deficient mice treated with AAV-ie-*Lphn2pr*-mCherry showed no significant improvements in any of the above parameters (Figure 6A-6D and Figure S7D). The mechanosensitive potentials of the LPHN2-expressing cochlear hair cells were also evaluated, and our results indicated that approximately 22% of the mCherry-labelled cochlear hair cells in AAV-ie-LPHN2-treated *Pou4f3-CreER*$^{+/-}$*Lphn2*$^{fl/fl}$ mice showed significantly increased current amplitude in response to force applied by LPHN2-M-beads, which was comparable to the proportion of force-sensitive cluster I hair cells in the WT mice (Figure 6E-6F and Figure S7E). In contrast, none of the cochlear hair cells labelled by the control virus

AAV-ie-*Lphn2pr*-mCherry in *Pou4f3-CreER*$^{+/-}$*Lphn2*$^{fl/fl}$ mice showed detectable force-induced excitability (Figure 6E-6F and Figure S7E). Collectively, these findings suggest that LPHN2 in cochlear hair cells directly contributes to auditory perception through the sensation of mechanical force.

Discussion

Cochlear hair cells convert sound stimuli into electrochemical signals through activation of MET channels. Despite decades of intensive efforts, the composition of the MET channels and the detailed mechanism underlying the MET process remain elusive. Because of the very rapid activation and ultralow response latency of cochlear hair cells in the submillisecond range, the MET process was conventionally believed to be directly regulated by ion channels but not by GPCRs, which usually transduce signals although second messengers or enzymatic pathways. In the present work and our parallel study, we showed that a mechanosensitive GPCR, LPHN2, can elicit MET in both utricle and cochlear hair cells by activating Gs-cAMP signalling, leading to positive modulation of membrane excitability after force sensation in both the auditory and vestibular systems. Notably, sensation of force by LPHN2 elicits a much faster Ca^{2+} response and membrane current change in cochlear hair cells than in utricular hair cells. These different time scales of LPHN2-regulated MET in these two systems may be related to the distinct expression patterns of LPHN2. Whereas LPHN2 is expressed at the cuticular plates of both utricle and cochlear hair cells, it shows a unique distribution along the stereocilia of the cochlear hair cells but not those of utricular hair cells. We therefore speculate that the different microenvironments within the stereocilia and the cuticular plate, such as the different cross-sectional areas (approximately 0.1 μm^2 and 19.6 μm^2 for stereocilia and the cuticular plate, respectively) and the potential compartmentalization with other signalling molecules, might affect the diffusion dynamics of cAMP downstream of LPHN2 activation, contributing to different time scales of LPHN2-mediated MET in the auditory and vestibular systems. Previous studies have suggested that the diffusion coefficients of cAMP in olfactory cilia, neonatal cardiac myocytes and neurons range from 136 to approximately 780 $\mu m^2/s$ (Bacskai et al., 1993; Chen et al., 1999; Neves et al., 2008; Nikolaev et al., 2004; Saucerman et al., 2006). If we assume that the cAMP

coefficient is similar in hair cells, then the theoretical time required for the transduction of the information of LPHN2-sensed force by cAMP is approximately 12.8 μs~73.5 μs in stereocilia and approximately 25.1~144 ms in the cuticular plate, which is partially consistent with the faster signals of LPHN2 in cochlear hair cells than in vestibular hair cells. Interestingly, we have noticed that both *Lphn2*$^{+/-}$ mice and *Pou4f3-CreER*$^{+/-}$*Lphn2*$^{fl/fl}$ mice show abnormal ABR wave I latency and amplitude compared with their respective control littermates, which happens within 2 ms after sound stimulation and is consistent with the theoretically calculated time latency of LPHN2-induced MET. However, both this theoretically calculated MET latency and the latency change caused by LPHN2 deficiency during the ABR tests are significantly shorter than our experimentally observed MET time after LPHN2 activation (~ 95ms). We therefore speculate several possibilities to reconcile these discrepancies: (1) the time latency caused by the linkage of LPHN2 antibody coated beads and LPHN2 receptor, as the force applied on the beads may take certain time to reach the receptor because of the flexible linker; (2) We measured MET under room temperature whereas the ABR experiments are performed under physiological temperature; (3) Sound sensing is a complicated process. Sound stimulation may activate multiple receptors at the same time but our magnetic beads only activate one receptor, which caused latency difference. Or LPHN2 might only be one of several critical components of the sound sensing complex. Importantly, application of force on the magnetic beads coated with specific antibody against protocadherin 15 or cadherin 23, which are central components of tip-link (Kazmierczak et al., 2007; Siemens et al., 2004; Sotomayor et al., 2012), induces a Ca^{2+} response in cochlear hair cells with a similar time latency (100 ~ 200 ms) to that recorded for LPHN2-M-beads (unpublished observation). The hair bundle deflection accompanied by the movement of tip-link has been hypothesized as the main driving force for the MET occurred at the stereocilia tips. Therefore, the comparable time latency recorded for the magnetic beads targeting LPHN2 and tip-link proteins suggests that the longer time latency via magnetic beads than in vivo ABR differences caused by LPHN2 deficiency is most likely due to the experimental conditions. These results also support the functional importance of LPHN2 comparable to the key component of the tip link during MET process. Clearly, further experimental condition optimizations, biophysics studies using super-resolution fluorescence imaging with highly sensitive cAMP sensors or

detailed mathematical calculations might be helpful for elucidating the mechanism underlying the dynamics of LPHN2-mediated MET.

Our work indicates that LPHN2 promotes MET in cochlear hair cells through Gs engagement, which elevates intracellular cAMP levels and positively regulates hair cell excitability. The LPHN2-mediated auditory MET is more similar to the signalling mechanism for smell perception than to that for visual perception, which relies mainly on the Gt-mediated inhibition of constitutive cGMP levels in photoreceptor cells. Consistent with our findings, cAMP has been proposed to modulate the sensitivity of the MET in cochlear hair cells (Mecca et al., 2022). Notably, a loss-of-function mutation in adenylyl cyclase 1 (AC1) caused by the deletion of the C-terminal 82 amino acids is linked to hearing loss in humans (Santos-Cortez et al., 2014). Moreover, AC1 was expressed at the stereocilia of cochlear hair cells, supporting our speculation that localized Gs-cAMP signalling plays important roles in auditory perception. The *Drosophila* LPHN homologue, Ca^{2+}-independent receptor of latrotoxin (Cirl), has been reported to respond to mechanical stimuli in vivo through interaction with the Toll-like receptor Tollo, which modulates the sensitivity of tactile and auditory stimuli in *Drosophila* (Scholz et al., 2023; Scholz et al., 2015). However, in contrast to the function of LPHN2 in cochlear hair cells, Cirl has been found to convert mechanical stimulation into a decrease in intracellular cAMP level in the sensory neurons of *Drosophila* (Scholz et al., 2017). However, the downstream ion channel of Cirl that putatively transmits the cAMP alteration into electrical signals remains unknown. Intriguingly, our parallel study also indicated that the other two LPHN subfamily members, LPHN1 and LPHN3, could activate Gi signalling in response to force stimulation but the heterozygous deficiency of single-receptor resulted in no obvious hearing loss phenotype (unpublished observation). Therefore, according to previous publications and our experimental results, mechanosensitive LPHNs and their homologues might represent one subfamily of evolutionally conserved auditory sensors that act through potentially different mechanisms in mammals and lower organisms. These differences might be the result of evolutionary adaptation to sound stimuli in more complex environments. In addition to LPHN2, we observed that VLGR1 was able to promote an intracellular cAMP increase in response to force sensation. Many VLGR1 mutants cause hearing loss, so we speculate that VLGR1 could be another candidate sound sensor in

cochlear hair cells.

Ion channels located at the tips of the stereocilia, such as TMC1 and TMC2, are proposed to be key components of the MET complex. Recent studies have also revealed the expression of the mechanosensitive protein Piezo2 at the cuticular plates of hair cells, where Piezo2 possibly functions as a subunit of the reverse-polarity channel (Wu et al., 2017). In the present study, we identified a novel regulatory role of the cation channel CNGA3 in the MET process and auditory perception. Our results suggest that CNGA3 is expressed at both the stereocilia and cuticular plates of cochlear hair cells, consistent with the localization of CNGA3 in saccular hair cells suggested by a previous study (Selvakumar et al., 2012). Importantly, the force sensation by LPHN2 is converted into rapid electoral signals in cochlear hair cells through coupling to CNGA3, and pharmacological inhibition of CNGA3 activity in mice severely impairs auditory functions. These findings not only support an essential role of the LPHN2-CNGA3 axis in hearing but also indicate that CNGA3 is a key component of the MET machinery. Moreover, we observed a direct association between LPHN2 and CNGA3 in vivo, which might shorten the diffusion time of cAMP, thus partially accounting for the fast signals of LPHN2-mediated MET. However, the detailed mechanism underlying the LPHN2-CNGA3 association and the potential contribution of this direct interaction to LPHN2-mediated MET require further studies, such as mutational analysis and gene knock-in mouse model studies. In addition, we found that LPHN2 was able to directly interact with TMC1 (Figure S5B). It will be of interest to further explore the potential contribution of the LPHN2-TMC1 interaction to the MET exerted by hair bundle deflection and to auditory perception in vivo. Collectively, our findings identify a force-sensitive aGPCR, LPHN2, that is essential for normal auditory perception and can sense force in cochlear hair cells and convert the force sensation into downstream CNGA3 activation and membrane depolarization. Both LPHN2 and CNGA3 are active components during MET processes in hair cells.

Author contributions

J.-P.S. and X.Y. initiated, designed and supervised the overall project. J.-P.S. conceived the idea of searching for MET-regulating GPCRs in the cochlear system at 2011 and initiated the screening process by collaborating with Z.-G.X.. X.Y. and C.W. designed and supervised all

electrophysiology experiments. Z.-G.X provided guidance and suggestions on the cochlear studies. Z.Y. and J.-P.S. developed the magnetic force stimulation assay to examine the activation of G proteins and second messengers downstream of GPCRs. Z.Y., M.-W.W., S.-H.Z. and Z.-C.S. performed the cell-based assay of LPHNs. Z.Y., Z.-C.S., M.-W.W., S.-H.Z. and J.-R.G. performed the electrophysiological experiments and Ca^{2+} imaging supervised by J.-P.S. and X.Y.. J.-P.S., Z.Y., M.-W.W. and S.-H.Z. participated in the design of gene knockout mice and modified AAV-ie. Z.Y., M.-W.W., Z.-C.S., Q.-Y.Z., W.-W.L. and L.X. performed cochlear behaviour studies. Z.Y., M.-W.W., and Z.-C.S. isolated mouse cochlea and performed immunofluorescence studies and ex vivo experiments. M.-W.W. and Z.-C.S. performed single cell qRT-PCR. M.-W.W. and Y. G. performed coimmunoprecipitation and western blotting analyses. Z.Y., M.-W.W., S.-H.Z., Z.-C.S., J.-R.G. and W.-W.L. performed the AAV-ie-related experiments. J.-P.S., X.Y., Z.-G.X, C.W., Z.Y., M.-W.W., S.-H.Z., Z.-C.S. and J.-R.G. participated in data analysis and interpretation. Z.-G.X., C.W., W.-W.L. and L.X. provided insightful ideas related to the auditory sensation. Z.Y., M.-W.W., S.-H.Z., Z.-C.S. and J.-R.G. prepared the figures. J.-P.S., X.Y., Z.Y., Z.-G.X and C.W. wrote the manuscript. All the authors have seen and commented on the manuscript.

Competing interests

The authors declare no competing interests.

Submission history

The manuscript was submitted on Sep 20th,2023 and was sent for peer review on Sep 26th , 2023 by the journal editor.

Figure legends

Figure 1. Expression of LPHN2 in cochlear hair cells

(A) mRNA levels of *Lphn2* in the cochlear epithelium isolated from WT mice at E20, P1, P7, P14, P30, P60, P120 and P240 (n = 6). Data are normalized to the mRNA levels of *Lphn2* at E20. E, embryonic period; P, postnatal day.

(B) Representative blotting showing the protein levels of LPHN2, Myosin7a (specific marker of hair cell body) and PCDH15 (specific marker of the stereocilia) in the stereocilia and cell body of cochlear or utricle hair cells isolated from WT mice at P10. Representative blotting from three independent experiments are shown (n = 3). LPHN2 antibody against the N terminus (551 - 600 residues) was used, which revealed both the full-length (~130 kDa) and the N-terminal fragment of LPHN2 (~120 kDa) in the cochlear or utricle hair cells. Data are correlated to Figure S1D-1E.

(C) Schematic diagram showing the expression pattern of LPHN2 in cochlear and utricle hair cells, respectively.

(D) Co-immunostaining of LPHN2 (green) and Phalloidin (red) in the stereocilia of OHC (left) and IHC (right) in cochlear whole mounts derived from WT mice at P30 (n = 6 mice per group). Scale bar, 5 μm. White arrows show the localization of LPHN2 at the tips of stereocilia. Data are correlated to Figure S1H.

(E) Co-immunostaining of LPHN2 (green) and Spectrin (red) at the cuticular plate of OHC (left) and IHC (right) in cochlear whole mounts derived from WT mice at P30 (n = 6 mice per group). Scale bar, 5 μm.

(F) Co-immunostaining of LPHN2 (green) and Myosin7a (red) in cochlear sections derived from WT mice at P30 (n = 6 mice per group). Scale bar, 20 μm. White arrows show the specific distribution of LPHN2 at the cuticular plate.

(A) *P < 0.05; ***P < 0.001. WT mice at P1, P7, P14, P30, P60, P120 and P240 compared with WT mice at E20. The bars indicate mean ± SEM values. All data were statistically analyzed using one-way ANOVA with Dunnett's post hoc test.

Figure 2. LPHN2 deficiency severely impairs hearing

(A-D) ABR thresholds (A), ABR waveforms at click (B), ABR peak1 (P1) latency (left) and amplitude (right) (C), and DPOAE thresholds (D) of WT and *Lphn2*$^{+/-}$ mice at P30 (n = 8 mice per group). ABR, auditory brainstem response; DPOAE, distortion product otoacoustic emission.

(E-H) ABR thresholds (E), ABR waveforms at click (F), ABR peak1 (P1) latency (left) and

amplitude (right) (G), and DPOAE thresholds (H) of *Pou4f3-CreER*$^{+/-}$*Lphn2*$^{+/+}$ (referred to as *Pc-Lphn2*$^{+/+}$) and *Pou4f3-CreER*$^{+/-}$*Lphn2*$^{fl/fl}$ (referred to as *Pc-Lphn2*$^{fl/fl}$) mice at P30 (n = 8 mice per group).

(I) Immunostaining of Myosin7a (red) in cochlear hair cells derived from *Pc-Lphn2*$^{+/+}$ and *Pc-Lphn2*$^{fl/fl}$ mice at P30 (n = 6 mice per group). Scale bar, 20 μm. Data are correlated to Figure S2K.

(J) Representative SEM images showing hair bundle morphology of the OHC (left) and IHC (right) from *Pc-Lphn2*$^{+/+}$ and *Pc-Lphn2*$^{fl/fl}$ mice at P30 (n = 6 mice per group). Scale bar, 1 μm (OHC) or 2 μm (IHC).

(A, C and D) **P < 0.01; ***P < 0.001; ns, no significant difference. *Lphn2*$^{+/-}$ mice compared with WT mice. (E, G and H) **P < 0.01; ***P < 0.001. *Pc-Lphn2*$^{fl/fl}$ mice compared with *Pc-Lphn2*$^{+/+}$ mice. The bars indicate mean ± SEM values. All data were statistically analyzed using two-way ANOVA with Dunnett's post hoc test.

Figure 3. Force sensation by LPHN2 induces cAMP and Ca^{2+} signals

(A) Endogenous cAMP level changes in the cochlea (apex, middle or base) and utricle explant derived from *Pc-Lphn2*$^{+/+}$ or *Pc-Lphn2*$^{fl/fl}$ mice at P10 in response to force (3 pN) applied by LPHN2-M-beads (n = 6). NF449 (10 μM), a specific Gs inhibitor.

(B) mRNA levels of different G protein subtypes in LPHN2-expressing cochlear hair cells derived from WT mice at P10 measured by single-cell qRT-PCR (n = 20 hair cells). The mRNA levels of respective G protein subtypes in the brain were used as the reference (normalized to 1).

(C) Heatmaps showing the Ca^{2+} responses in LPHN2-expressing cochlear hair cells derived from P10 *Pc-Lphn2*$^{+/+}$ mice labelled by AAV-ie-*Lphn2pr*-mCherry (n = 60 hair cells). The vertical yellow full line denotes the onset of force application (0 s). Each row represents the temporal Ca^{2+} response of one hair cell. Data are correlated to Figure 3D-3E and Figure S3E-3F.

(D) Representative Ca^{2+} traces recorded in individual cochlear hair cells derived from P10 *Pc-Lphn2*$^{+/+}$ mice labelled by AAV-ie-*Lphn2pr*-mCherry. Data are correlated to Figure 3C and

Figure S3E-3F.

(E) Proportion of force-sensitive and force-insensitive cochlear hair cells derived from P10 *Pc-Lphn2*$^{+/+}$ mice labelled by AAV-ie-*Lphn2pr*-mCherry. Data are correlated to Figure 3C-3D and Figure S3E-3F.

(F) Effects of Gs inhibitor NF449 (10 μM), Gq inhibitor YM-254890 (60 μM) and Ca^{2+}-free buffer on the force-induced Ca^{2+} responses in cochlear hair cells labelled by AAV-ie-*Lphn2pr*-mCherry (n = 10 hair cells per group). Data are correlated to Figure S3G-3I.

(G) Dose-dependent inhibitory effects of NF449 treatment on force-stimulated Ca^{2+} responses in cochlear hair cells labelled by AAV-ie-*Lphn2pr*-mCherry (n = 18 hair cells). Data are correlated to Figure S3K.

Figure 4. Force sensation by LPHN2 elicits acute currents in cochlear hair cells

(A-B) Representative whole-cell currents (upper panel) elicited by voltage steps between -100 mV and +100 mV and the corresponding I-V curves (lower panel) in AAV-ie-*Lphn2pr*-mCherry-labeled cluster I (A) or cluster II (B) cochlear hair cells derived from *Pc-Lphn2*$^{+/+}$ or *Pc-Lphn2*$^{fl/fl}$ mice in response to force (3 pN) stimulation. N = 15 for cluster I cells and n = 50 for cluster II cells in *Pc-Lphn2*$^{+/+}$ mice. N = 10 for cluster I cells and n = 30 for cluster II cells in *Pc-Lphn2*$^{fl/fl}$ mice. Data are correlated to Figure S4A.

(C) Representative force-induced membrane potential alteration of cluster I cochlear hair cells derived from *Pc-Lphn2*$^{+/+}$ mice when holding at absolute zero current (n = 10 hair cells). The time latency between force application or force removal and the change of membrane potential was defined as T_{pr} and T_{po}, respectively. The calculated time for recovery time constant was denoted as τ_{rec}.

(D) The calculated time parameters in force-stimulated membrane potential alteration of *Pc-Lphn2*$^{+/+}$ cluster I cochlear hair cells (n = 10 hair cells). Data are correlated to Figure 4C.

(E) Effect of NF449 treatment on the whole-cell current in *Pc-Lphn2*$^{+/+}$ cluster I hair cells in response to 3 pN force stimulation (n = 6 hair cells). Data are correlated to Figure S4C-4D.

(F) Effect of NF449 treatment on the force-stimulated membrane potential alteration in *Pc-Lphn2*$^{+/+}$ cluster I hair cells (n = 6 hair cells). Data are correlated to Figure S4C-4D.

(G) Schematic diagram showing the different latency time of the force-induced current

responses through activating LPHN2 in cochlear (upper panel, ~95 ms) or utricle (lower panel, ~705 ms) hair cells.

(H) Force (3 pN)-induced FM1-43 (green) uptake in cochlea explant derived from P10 *Pc-Lphn2*$^{+/+}$ or *Pc-Lphn2*$^{fl/fl}$ mice within 5 sec at the presence or absence of NF449 (n = 6 per group). Data are correlated to Figure S4E.

Figure 5. LPHN2 regulates MET in cochlear hair cells through coupling to CNGA3 cells

(A) mRNA levels of CNG and HCN channels in WT cluster I and cluster II cochlear hair cells examined by single-cell qRT-PCR (n = 10 cells per cluster). The mRNA levels of these ion channels in the brain were used as the reference (normalized to 1).

(B) Representative blotting showing the co-immunoprecipitation of LPHN2 with CNGA3 channel in the lysates of mouse cochlea. Representative blotting form three independent experiments are shown (n = 3). Data are correlated to Figure S5B.

(C) Co-immunostaining of LPHN2 (green), CNGA3 (magenta) and phalloidin (red) in cochlea sections derived from WT mice at P30 (n = 6 mice per group). Scale bar: 5 μm. White arrows show co-localization of LPHN2 and CNGA3 at the stereocilia and cuticular plate.

(D-E) ABR thresholds (D) and DPOAE thresholds (E) of *Pou4f3-CreER*$^{+/-}$*Cnga3*$^{+/+}$ (referred to as *Pc-Cnga3*$^{+/+}$) and *Pou4f3-CreER*$^{+/-}$*Cnga3*$^{fl/+}$ (referred to *Pc-Cnga3*$^{fl/+}$) mice at P30 (n = 8 mice per group). Data are correlated to Figure S5G-5H.

(F-G) Representative traces (F) and the dose-response curve (G) showing the effect of CNG inhibitor L-cis-diltiazem on the force (3 pN)-induced Ca^{2+} responses in individual cochlear hair cell derived from P10 *Pc-Cnga3*$^{+/+}$ cluster I hair cells (n = 18 hair cells). Data are correlated to Figure S5I.

(H-I) Representative I-V curves (H) and the dose-response curve (I) showing the effect of L-cis-diltiazem on the force (3 pN)-induced the whole-cell current in individual cochlear hair cell derived from P10 *Pc-Cnga3*$^{+/+}$ cluster I hair cells (n = 6 hair cells). Data are correlated to Figure S5J.

(J-K) Representative fluorescence images (J) and quantification analysis (K) of the effect of L-cis-diltiazem treatment on the force (3 pN)-induced FM1-43 uptake in cochlea explant derived from P10 *Pc-Cnga3*$^{+/+}$ mice within 5 sec (n = 6 mice per group).

(D-E) ***P < 0.001; ns, no significant difference. *Pc-Cnga3*$^{fl/+}$ mice compared with *Pc-Cnga3*$^{+/+}$ mice at P30. (K) **P < 0.01; ***P < 0.001. Cochlea explants treated with force compared with the control. $^{###}$P < 0.001. Cochlea explants treated with L-cis-diltiazem compared with those treated with control vehicle. The bars indicate mean ± SEM values. All data were statistically analyzed using two-way ANOVA with Dunnett's post hoc test.

Figure 6. LPHN2 re-expression in cochlear hair cells of *Lphn2*-deficient mice rescues hearing loss

(A-D) ABR thresholds (A), ABR peak1 (P1) latency (B) and amplitude (C), and DPOAE thresholds (D) of *Pc-Lphn2*$^{+/+}$, *Pc-Lphn2*$^{fl/fl}$, AAV-ie-*Lphn2pr*-LPHN2-mCherry-treated *Pc-Lphn2*$^{fl/fl}$ mice (referred to as AAV-ie-LPHN2 mice) and AAV-ie-*Lphn2pr*-mCherry-treated *Pc-Lphn2*$^{fl/fl}$ mice (referred to as AAV-ie-*Lphn2pr* mice) at P30 (n = 6 mice per group). Data are correlated to Figure S7D.

(E) Representative whole-cell currents (left) elicited by voltage steps between -100 mV and +100 mV and the corresponding I-V curves (right) in cluster I cochlear hair cells derived from *Pc-Lphn2*$^{+/+}$, AAV-ie-LPHN2 and AAV-ie-*Lphn2pr* mice in response to force (3 pN) stimulation (n = 5 ~ 6 hair cells per group). Data are correlated to Figure S7E.

(F) Quantification of force-sensitive and force-insensitive cochlear hair cells derived from *Pc-Lphn2*$^{+/+}$, AAV-ie-LPHN2 and AAV-ie-*Lphn2pr* mice. Data are correlated to Figure 6E.

(A-D) **P < 0.01; ***P < 0.001; ns, no significant difference. *Pc-Lphn2*$^{fl/fl}$, AAV-ie-LPHN2 or AAV-ie-*Lphn2pr* mice compared with *Pc-Lphn2*$^{+/+}$ mice. The bars indicate mean ± SEM values. All data were statistically analyzed using one-way ANOVA with Dunnett's post hoc test.

References

Anderson, G.R., Maxeiner, S., Sando, R., Tsetsenis, T., Malenka, R.C., and Sudhof, T.C.

658 (2017). Postsynaptic adhesion GPCR latrophilin-2 mediates target recognition in entorhinal-
659 hippocampal synapse assembly. J Cell Biol *216*, 3831-3846.
660 Avenarius, M.R., Krey, J.F., Dumont, R.A., Morgan, C.P., Benson, C.B., Vijayakumar, S.,
661 Cunningham, C.L., Scheffer, D.I., Corey, D.P., Muller, U.*, et al.* (2017). Heterodimeric capping
662 protein is required for stereocilia length and width regulation. J Cell Biol *216*, 3861-3881.
663 Bacskai, B.J., Hochner, B., Mahaut-Smith, M., Adams, S.R., Kaang, B.K., Kandel, E.R., and
664 Tsien, R.Y. (1993). Spatially resolved dynamics of cAMP and protein kinase A subunits in
665 Aplysia sensory neurons. Science *260*, 222-226.
666 Buck, L., and Axel, R. (1991). A novel multigene family may encode odorant receptors: a
667 molecular basis for odor recognition. Cell *65*, 175-187.
668 Chen, C., Nakamura, T., and Koutalos, Y. (1999). Cyclic AMP diffusion coefficient in frog
669 olfactory cilia. Biophys J *76*, 2861-2867.
670 Cunningham, C.L., Qiu, X., Wu, Z., Zhao, B., Peng, G., Kim, Y.H., Lauer, A., and Muller, U.
671 (2020). TMIE Defines Pore and Gating Properties of the Mechanotransduction Channel of
672 Mammalian Cochlear Hair Cells. Neuron *107*, 126-143 e128.
673 Douguet, D., and Honore, E. (2019). Mammalian Mechanoelectrical Transduction: Structure
674 and Function of Force-Gated Ion Channels. Cell *179*, 340-354.
675 Duncan, J.S., Stoller, M.L., Francl, A.F., Tissir, F., Devenport, D., and Deans, M.R. (2017).
676 Celsr1 coordinates the planar polarity of vestibular hair cells during inner ear development.
677 Dev Biol *423*, 126-137.
678 Filipek, S., Stenkamp, R.E., Teller, D.C., and Palczewski, K. (2003). G protein-coupled
679 receptor rhodopsin: a prospectus. Annu Rev Physiol *65*, 851-879.

680 Guan, Y., Du, H.B., Yang, Z., Wang, Y.Z., Ren, R., Liu, W.W., Zhang, C., Zhang, J.H., An,
681 W.T., Li, N.N., *et al.* (2023). Deafness-Associated ADGRV1 Mutation Impairs USH2A Stability
682 through Improper Phosphorylation of WHRN and WDSUB1 Recruitment. Adv Sci (Weinh) *10*,
683 e2205993.
684 Guo, L., Cheng, J., Lian, S., Liu, Q., Lu, Y., Zheng, Y., Zhu, K., Zhang, M., Kong, Y., Zhang,
685 C., *et al.* (2023). Structural basis of amine odorant perception by a mammal olfactory receptor.
686 Nature *618*, 193-200.
687 Jeong, H., Clark, S., Goehring, A., Dehghani-Ghahnaviyeh, S., Rasouli, A., Tajkhorshid, E.,
688 and Gouaux, E. (2022). Structures of the TMC-1 complex illuminate mechanosensory
689 transduction. Nature *610*, 796-803.
690 Jia, Y., Zhao, Y., Kusakizako, T., Wang, Y., Pan, C., Zhang, Y., Nureki, O., Hattori, M., and
691 Yan, Z. (2020). TMC1 and TMC2 Proteins Are Pore-Forming Subunits of Mechanosensitive
692 Ion Channels. Neuron *105*, 310-321 e313.
693 Jung, J., and Muller, U. (2023). Mechanoelectrical transduction-related genetic forms of
694 hearing loss. Curr Opin Physiol *32*.
695 Kaupp, U.B. (2010). Olfactory signalling in vertebrates and insects: differences and
696 commonalities. Nat Rev Neurosci *11*, 188-200.
697 Kazmierczak, P., Sakaguchi, H., Tokita, J., Wilson-Kubalek, E.M., Milligan, R.A., Muller, U.,
698 and Kachar, B. (2007). Cadherin 23 and protocadherin 15 interact to form tip-link filaments in
699 sensory hair cells. Nature *449*, 87-91.
700 Liang, X., Qiu, X., Dionne, G., Cunningham, C.L., Pucak, M.L., Peng, G., Kim, Y.H., Lauer, A.,
701 Shapiro, L., and Muller, U. (2021). CIB2 and CIB3 are auxiliary subunits of the

702 mechanotransduction channel of hair cells. Neuron *109*, 2131-2149 e2115.

703 Mecca, A.A., Caprara, G.A., and Peng, A.W. (2022). cAMP and voltage modulate rat auditory
704 mechanotransduction by decreasing the stiffness of gating springs. Proc Natl Acad Sci U S A
705 *119*, e2107567119.

706 Neves, S.R., Tsokas, P., Sarkar, A., Grace, E.A., Rangamani, P., Taubenfeld, S.M., Alberini,
707 C.M., Schaff, J.C., Blitzer, R.D., Moraru, II*, et al.* (2008). Cell shape and negative links in
708 regulatory motifs together control spatial information flow in signaling networks. Cell *133*, 666-
709 680.

710 Nikolaev, V.O., Bunemann, M., Hein, L., Hannawacker, A., and Lohse, M.J. (2004). Novel
711 single chain cAMP sensors for receptor-induced signal propagation. J Biol Chem *279*, 37215-
712 37218.

713 Pan, B., Akyuz, N., Liu, X.P., Asai, Y., Nist-Lund, C., Kurima, K., Derfler, B.H., Gyorgy, B.,
714 Limapichat, W., Walujkar, S.*, et al.* (2018). TMC1 Forms the Pore of Mechanosensory
715 Transduction Channels in Vertebrate Inner Ear Hair Cells. Neuron *99*, 736-753 e736.

716 Pan, B., Geleoc, G.S., Asai, Y., Horwitz, G.C., Kurima, K., Ishikawa, K., Kawashima, Y.,
717 Griffith, A.J., and Holt, J.R. (2013). TMC1 and TMC2 are components of the
718 mechanotransduction channel in hair cells of the mammalian inner ear. Neuron *79*, 504-515.

719 Ranum, P.T., Goodwin, A.T., Yoshimura, H., Kolbe, D.L., Walls, W.D., Koh, J.Y., He, D.Z.Z.,
720 and Smith, R.J.H. (2019). Insights into the Biology of Hearing and Deafness Revealed by
721 Single-Cell RNA Sequencing. Cell Rep *26*, 3160-3171 e3163.

722 Santos-Cortez, R.L., Lee, K., Giese, A.P., Ansar, M., Amin-Ud-Din, M., Rehn, K., Wang, X.,
723 Aziz, A., Chiu, I., Hussain Ali, R.*, et al.* (2014). Adenylate cyclase 1 (ADCY1) mutations cause

724 recessive hearing impairment in humans and defects in hair cell function and hearing in
725 zebrafish. Hum Mol Genet *23*, 3289-3298.
726 Saucerman, J.J., Zhang, J., Martin, J.C., Peng, L.X., Stenbit, A.E., Tsien, R.Y., and
727 McCulloch, A.D. (2006). Systems analysis of PKA-mediated phosphorylation gradients in live
728 cardiac myocytes. Proc Natl Acad Sci U S A *103*, 12923-12928.
729 Scholz, N., Dahse, A.K., Kemkemer, M., Bormann, A., Auger, G.M., Vieira Contreras, F.,
730 Ernst, L.F., Staake, H., Korner, M.B., Buhlan, M.*, et al.* (2023). Molecular sensing of
731 mechano- and ligand-dependent adhesion GPCR dissociation. Nature *615*, 945-953.
732 Scholz, N., Gehring, J., Guan, C., Ljaschenko, D., Fischer, R., Lakshmanan, V., Kittel, R.J.,
733 and Langenhan, T. (2015). The adhesion GPCR latrophilin/CIRL shapes mechanosensation.
734 Cell Rep *11*, 866-874.
735 Scholz, N., Guan, C., Nieberler, M., Grotemeyer, A., Maiellaro, I., Gao, S., Beck, S., Pawlak,
736 M., Sauer, M., Asan, E.*, et al.* (2017). Mechano-dependent signaling by Latrophilin/CIRL
737 quenches cAMP in proprioceptive neurons. Elife *6*.
738 Selvakumar, D., Drescher, M.J., Dowdall, J.R., Khan, K.M., Hatfield, J.S., Ramakrishnan,
739 N.A., and Drescher, D.G. (2012). CNGA3 is expressed in inner ear hair cells and binds to an
740 intracellular C-terminus domain of EMILIN1. Biochem J *443*, 463-476.
741 Shi, F., Hu, L., and Edge, A.S. (2013). Generation of hair cells in neonatal mice by beta-
742 catenin overexpression in Lgr5-positive cochlear progenitors. Proc Natl Acad Sci U S A *110*,
743 13851-13856.
744 Siemens, J., Lillo, C., Dumont, R.A., Reynolds, A., Williams, D.S., Gillespie, P.G., and Muller,
745 U. (2004). Cadherin 23 is a component of the tip link in hair-cell stereocilia. Nature *428*, 950-

746 955.

747 Smith, S.O. (2023). Mechanism of Activation of the Visual Receptor Rhodopsin. Annu Rev
748 Biophys *52*, 301-317.

749 Sotomayor, M., Weihofen, W.A., Gaudet, R., and Corey, D.P. (2012). Structure of a force-
750 conveying cadherin bond essential for inner-ear mechanotransduction. Nature *492*, 128-132.

751 Tan, F., Chu, C., Qi, J., Li, W., You, D., Li, K., Chen, X., Zhao, W., Cheng, C., Liu, X.*, et al.*
752 (2019). AAV-ie enables safe and efficient gene transfer to inner ear cells. Nat Commun *10*,
753 3733.

754 Tang, Y.Q., Lee, S.A., Rahman, M., Vanapalli, S.A., Lu, H., and Schafer, W.R. (2020).
755 Ankyrin Is An Intracellular Tether for TMC Mechanotransduction Channels. Neuron *107*, 112-
756 125 e110.

757 Wang, Y., Guo, N., and Nathans, J. (2006). The role of Frizzled3 and Frizzled6 in neural tube
758 closure and in the planar polarity of inner-ear sensory hair cells. J Neurosci *26*, 2147-2156.

759 Wu, Z., Grillet, N., Zhao, B., Cunningham, C., Harkins-Perry, S., Coste, B., Ranade, S.,
760 Zebarjadi, N., Beurg, M., Fettiplace, R.*, et al.* (2017). Mechanosensory hair cells express two
761 molecularly distinct mechanotransduction channels. Nat Neurosci *20*, 24-33.

762 Xiong, W., Grillet, N., Elledge, H.M., Wagner, T.F., Zhao, B., Johnson, K.R., Kazmierczak, P.,
763 and Muller, U. (2012). TMHS is an integral component of the mechanotransduction machinery
764 of cochlear hair cells. Cell *151*, 1283-1295.

765 Yang, F., Guo, L., Li, Y., Wang, G., Wang, J., Zhang, C., Fang, G.X., Chen, X., Liu, L., Yan,
766 X.*, et al.* (2021). Structure, function and pharmacology of human itch receptor complexes.
767 Nature *600*, 164-169.

768 Yang, Z., Cheng, J., Shang, P., Sun, J.P., and Yu, X. (2023). Emerging roles of olfactory
769 receptors in glucose metabolism. Trends Cell Biol *33*, 463-476.
770 Yau, K.W., and Hardie, R.C. (2009). Phototransduction motifs and variations. Cell *139*, 246-
771 264.
772 Zhang, Y., Hoon, M.A., Chandrashekar, J., Mueller, K.L., Cook, B., Wu, D., Zuker, C.S., and
773 Ryba, N.J. (2003). Coding of sweet, bitter, and umami tastes: different receptor cells sharing
774 similar signaling pathways. Cell *112*, 293-301.
775 Zheng, W., and Holt, J.R. (2021). The Mechanosensory Transduction Machinery in Inner Ear
776 Hair Cells. Annu Rev Biophys *50*, 31-51.
777

Figure 1

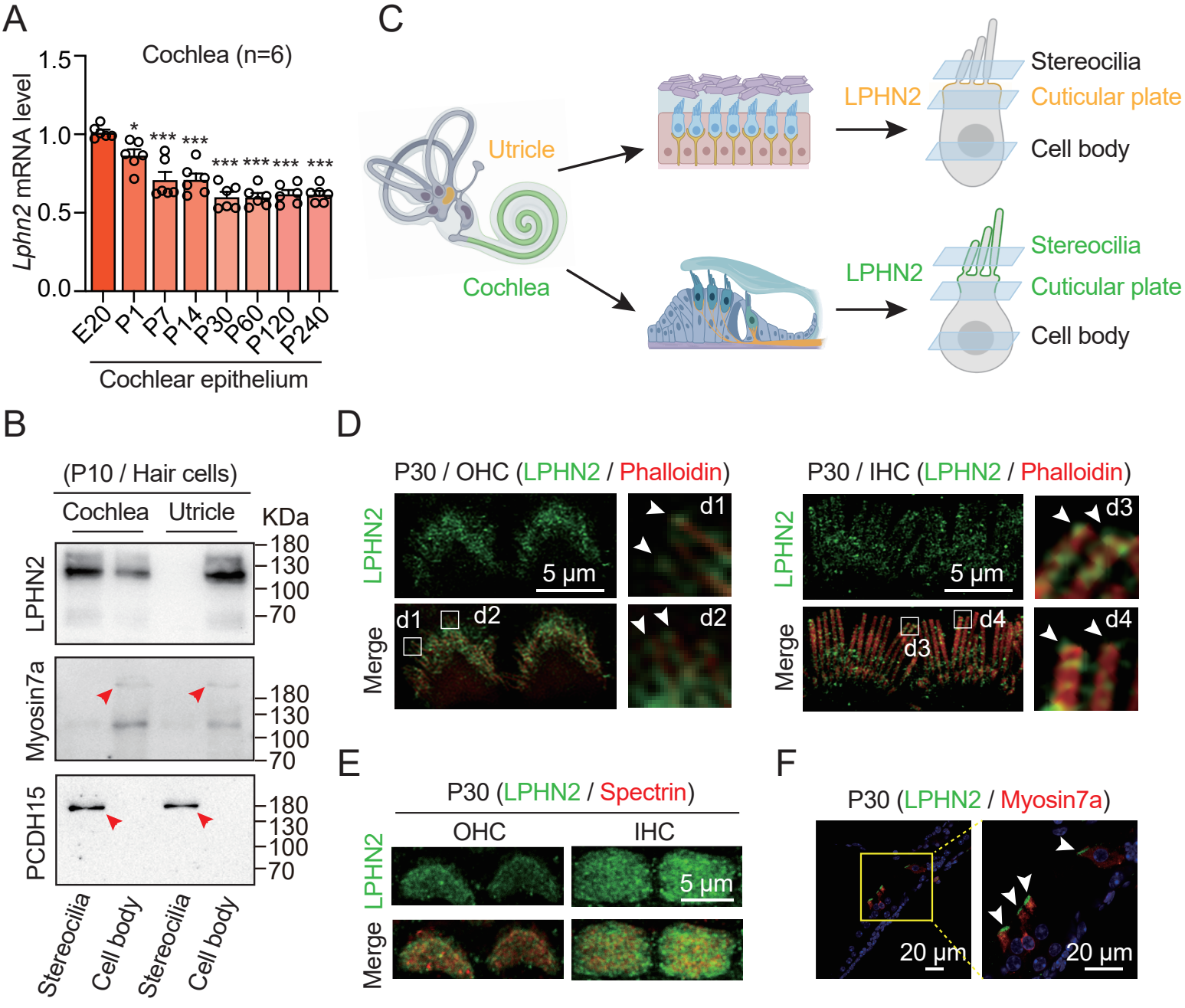
A
Cochlea (n=6)
Lphn2 mRNA level
1.5
1.0
0.5
0.0
*
***
E20
P1
P7
P14
P30
P60
P120
P240
Cochlear epithelium
C
Utricle
Cochlea
LPHN2
Stereocilia
Cuticular plate
Cell body
B
(P10 / Hair cells)
Cochlea
Utricle
KDa
LPHN2
Myosin7a
PCDH15
180
130
100
70
Stereocilia
Cell body
D
P30 / OHC (LPHN2 / Phalloidin)
P30 / IHC (LPHN2 / Phalloidin)
Merge
5 μm
d1
d2
d3
d4
E
P30 (LPHN2 / Spectrin)
OHC
IHC
F
P30 (LPHN2 / Myosin7a)
20 μm

Figure 2

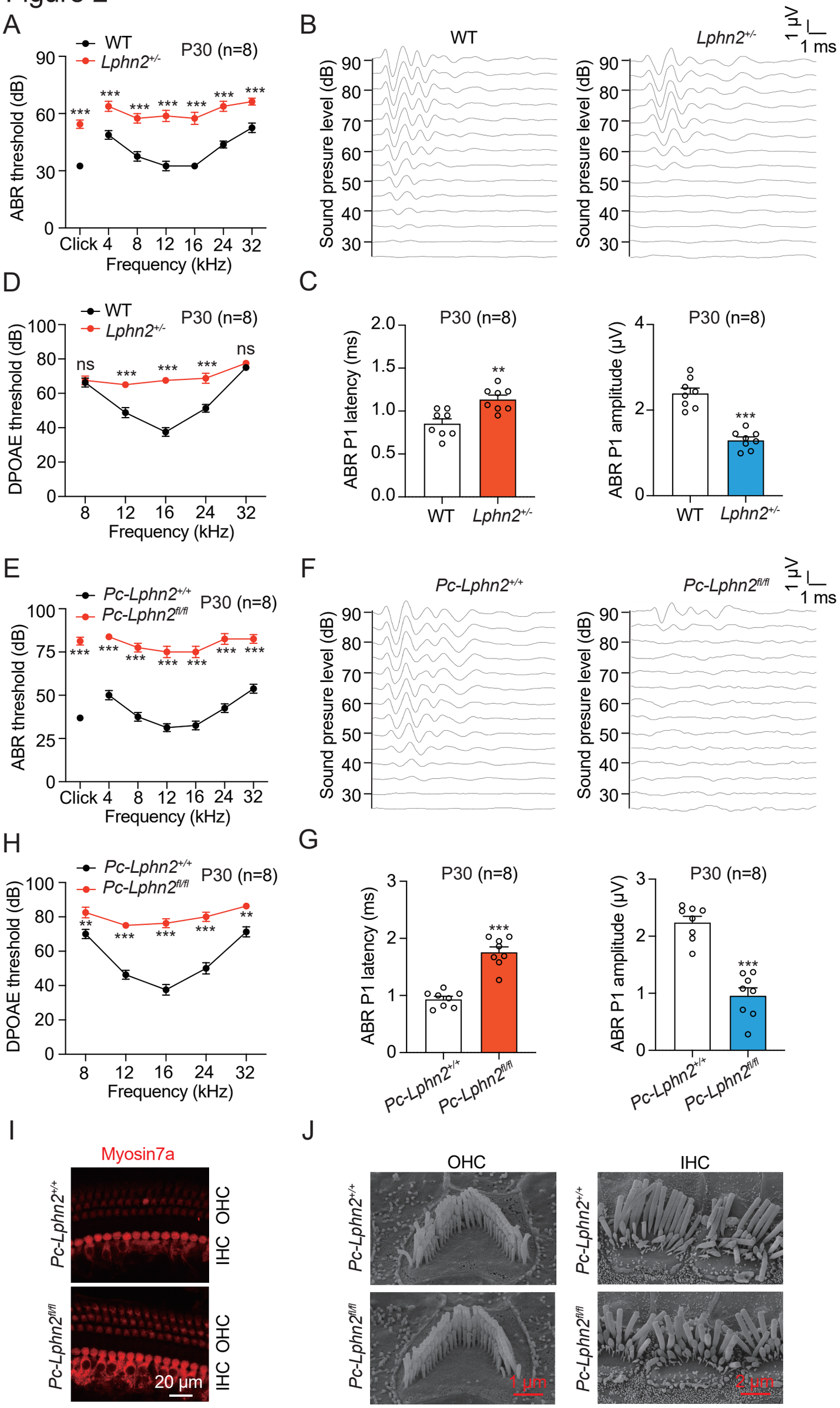
A
WT
Lphn2+/-
P30 (n=8)
ABR threshold (dB)
Click 4 8 12 16 24 32
Frequency (kHz)
B
WT
Lphn2+/-
1 μV
1 ms
Sound presure level (dB)
D
WT
Lphn2+/-
P30 (n=8)
DPOAE threshold (dB)
ns
Frequency (kHz)
C
P30 (n=8)
ABR P1 latency (ms)
ABR P1 amplitude (μV)
WT
Lphn2+/-
E
Pc-Lphn2+/+
Pc-Lphn2fl/fl
P30 (n=8)
ABR threshold (dB)
Click 4 8 12 16 24 32
Frequency (kHz)
F
Pc-Lphn2+/+
Pc-Lphn2fl/fl
1 μV
1 ms
Sound presure level (dB)
H
Pc-Lphn2+/+
Pc-Lphn2fl/fl
P30 (n=8)
DPOAE threshold (dB)
Frequency (kHz)
G
P30 (n=8)
ABR P1 latency (ms)
ABR P1 amplitude (μV)
Pc-Lphn2+/+
Pc-Lphn2fl/fl
I
Myosin7a
Pc-Lphn2+/+
Pc-Lphn2fl/fl
OHC
IHC
20 μm
J
OHC
IHC
Pc-Lphn2+/+
Pc-Lphn2fl/fl
1 μm
2 μm

Figure 3

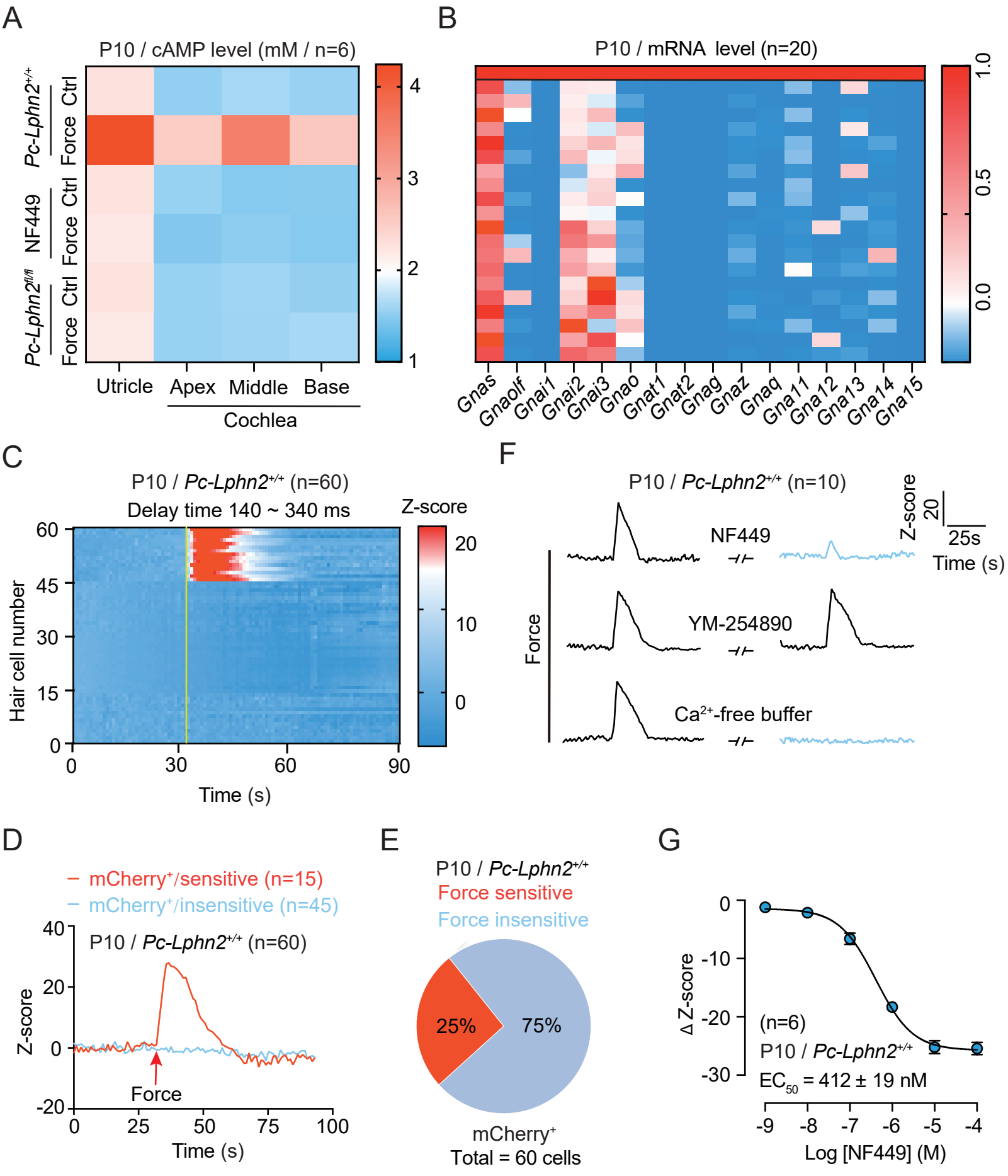
A
P10 / cAMP level (mM / n=6)
Pc-Lphn2+/+
Ctrl
Force
NF449
Ctrl
Force
Pc-Lphn2fl/fl
Ctrl
Force
Utricle
Apex
Middle
Base
Cochlea
4
3
2
1
B
P10 / mRNA level (n=20)
1.0
0.5
0.0
Gnas
Gnaolf
Gnai1
Gnai2
Gnai3
Gnao
Gnat1
Gnat2
Gnag
Gnaz
Gnaq
Gna11
Gna12
Gna13
Gna14
Gna15
C
P10 / Pc-Lphn2+/+ (n=60)
Delay time 140 ~ 340 ms
Z-score
20
10
0
Hair cell number
60
45
30
15
0
0
30
60
90
Time (s)
F
P10 / Pc-Lphn2+/+ (n=10)
Z-score
20
25s
Time (s)
NF449
YM-254890
Ca2+-free buffer
Force
D
mCherry+/sensitive (n=15)
mCherry+/insensitive (n=45)
P10 / Pc-Lphn2+/+ (n=60)
Z-score
40
20
0
-20
Force
0
25
50
75
100
Time (s)
E
P10 / Pc-Lphn2+/+
Force sensitive
Force insensitive
25%
75%
mCherry+
Total = 60 cells
G
0
-10
-20
-30
Δ Z-score
(n=6)
P10 / Pc-Lphn2+/+
EC50 = 412 ± 19 nM
-9
-8
-7
-6
-5
-4
Log [NF449] (M)

Figure 4

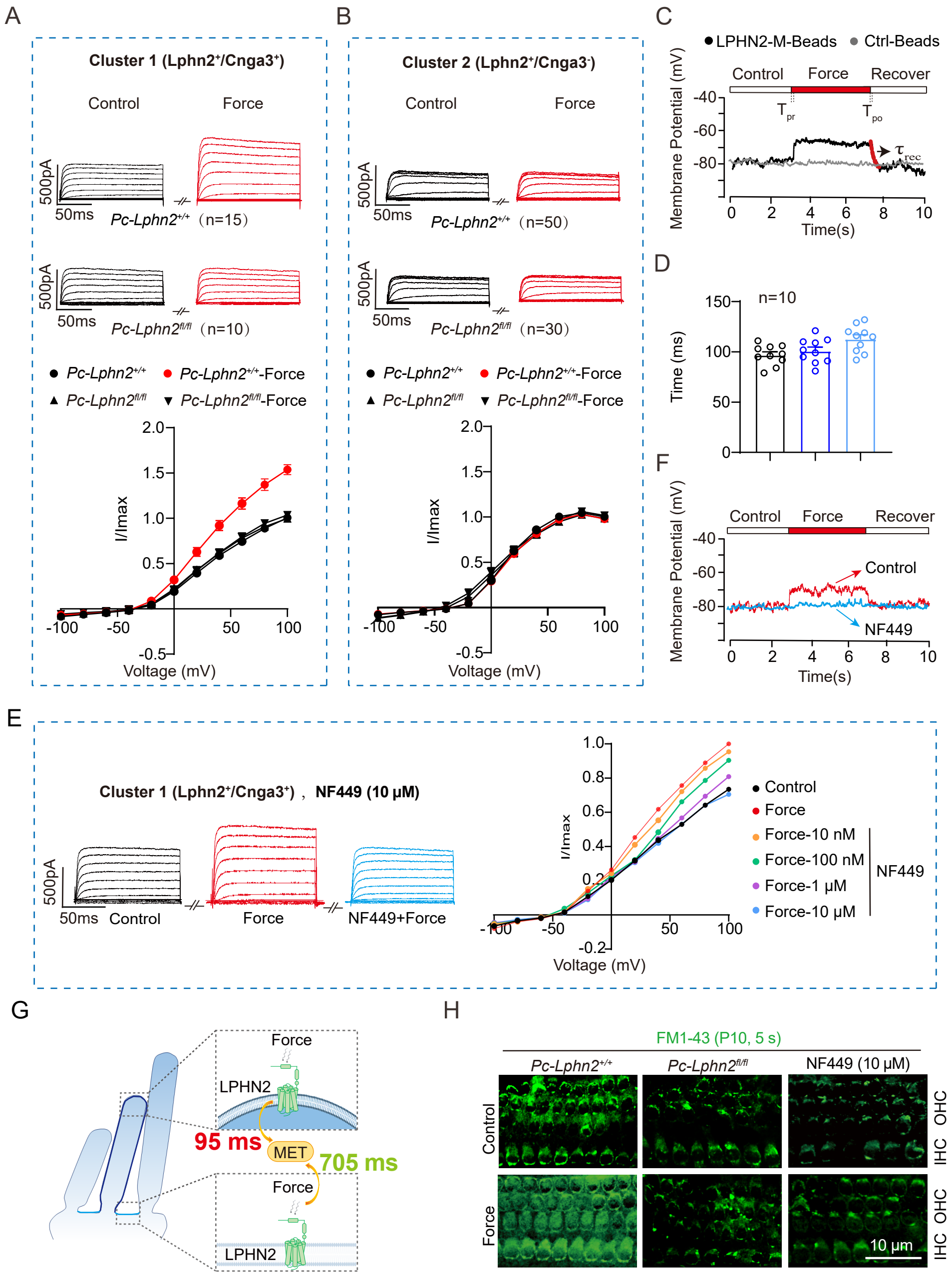
A
Cluster 1 (Lphn2+/Cnga3+)
Control
Force
500pA
50ms
Pc-Lphn2+/+ (n=15)
Pc-Lphn2fl/fl (n=10)
Pc-Lphn2+/+
Pc-Lphn2+/+-Force
Pc-Lphn2fl/fl
Pc-Lphn2fl/fl-Force
I/Imax
Voltage (mV)
B
Cluster 2 (Lphn2+/Cnga3-)
Pc-Lphn2+/+ (n=50)
Pc-Lphn2fl/fl (n=30)
C
LPHN2-M-Beads
Ctrl-Beads
Recover
Membrane Potential (mV)
Time(s)
D
n=10
Time (ms)
F
Control
NF449
E
Cluster 1 (Lphn2+/Cnga3+) , NF449 (10 μM)
Force
NF449+Force
Force-10 nM
Force-100 nM
Force-1 μM
Force-10 μM
NF449
G
LPHN2
95 ms
MET
705 ms
H
FM1-43 (P10, 5 s)
NF449 (10 μM)
OHC
IHC
10 μm

Figure 5

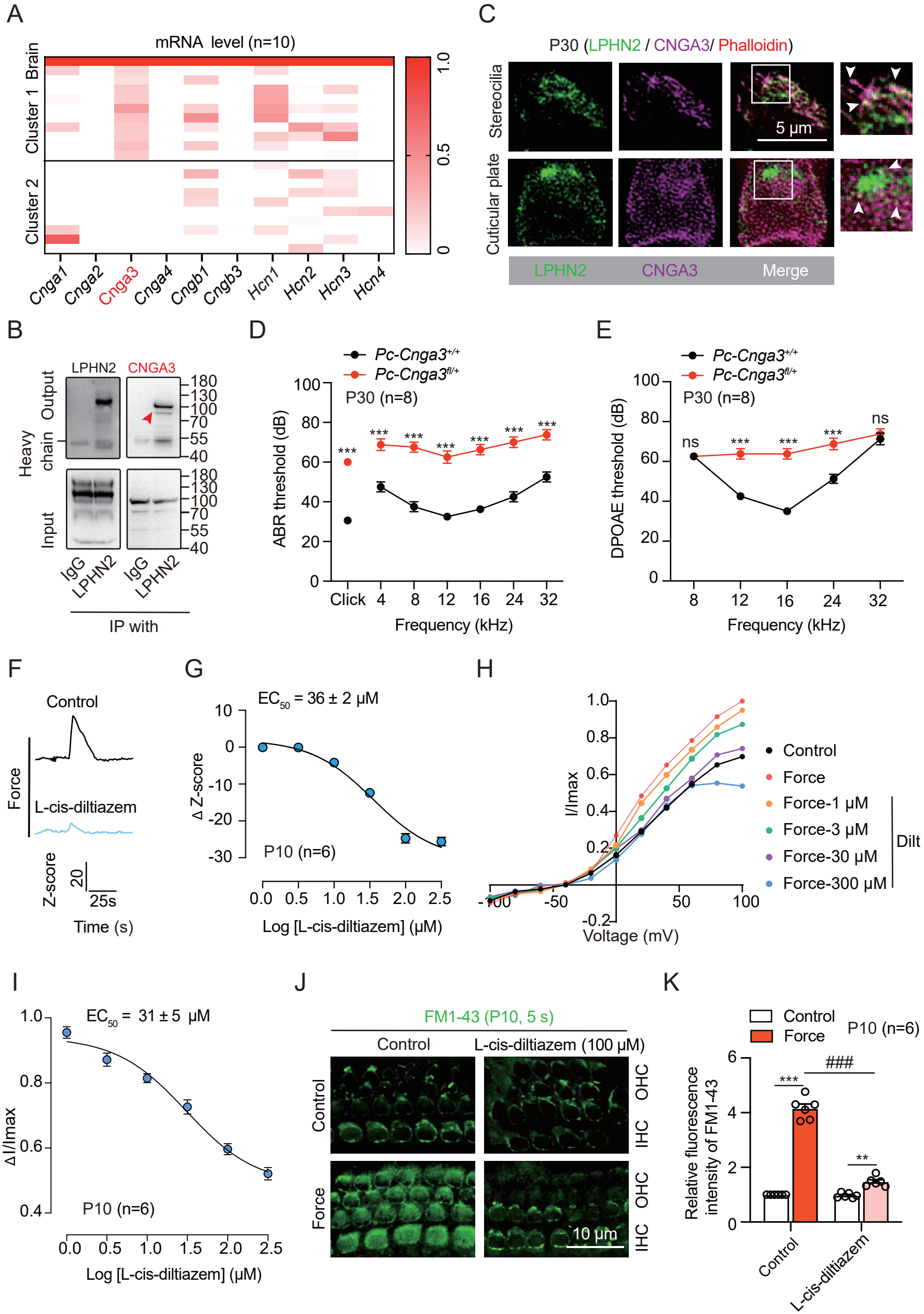
A
mRNA level (n=10)
Brain
Cluster 1
Cluster 2
1.0
0.5
0
Cnga1
Cnga2
Cnga3
Cnga4
Cngb1
Cngb3
Hcn1
Hcn2
Hcn3
Hcn4
C
P30 (LPHN2 / CNGA3/ Phalloidin)
Stereocilia
Cuticular plate
5 µm
LPHN2
CNGA3
Merge
B
LPHN2
CNGA3
Heavy chain
Output
Input
180
130
100
70
55
40
IgG
LPHN2
IP with
D
Pc-Cnga3+/+
Pc-Cnga3fl/+
P30 (n=8)
ABR threshold (dB)
Click
4
8
12
16
24
32
Frequency (kHz)
E
Pc-Cnga3+/+
Pc-Cnga3fl/+
P30 (n=8)
DPOAE threshold (dB)
ns
Frequency (kHz)
F
Control
Force
L-cis-diltiazem
Z-score
20
25s
Time (s)
G
EC50 = 36 ± 2 µM
Δ Z-score
P10 (n=6)
Log [L-cis-diltiazem] (µM)
H
I/Imax
Voltage (mV)
Control
Force
Force-1 µM
Force-3 µM
Force-30 µM
Force-300 µM
Dilt
I
EC50 = 31 ± 5 µM
ΔI/Imax
P10 (n=6)
Log [L-cis-diltiazem] (µM)
J
FM1-43 (P10, 5 s)
Control
L-cis-diltiazem (100 µM)
Control
Force
OHC
IHC
10 µm
K
Control
Force
P10 (n=6)
Relative fluorescence intensity of FM1-43
###
**
Control
L-cis-diltiazem

Figure 6

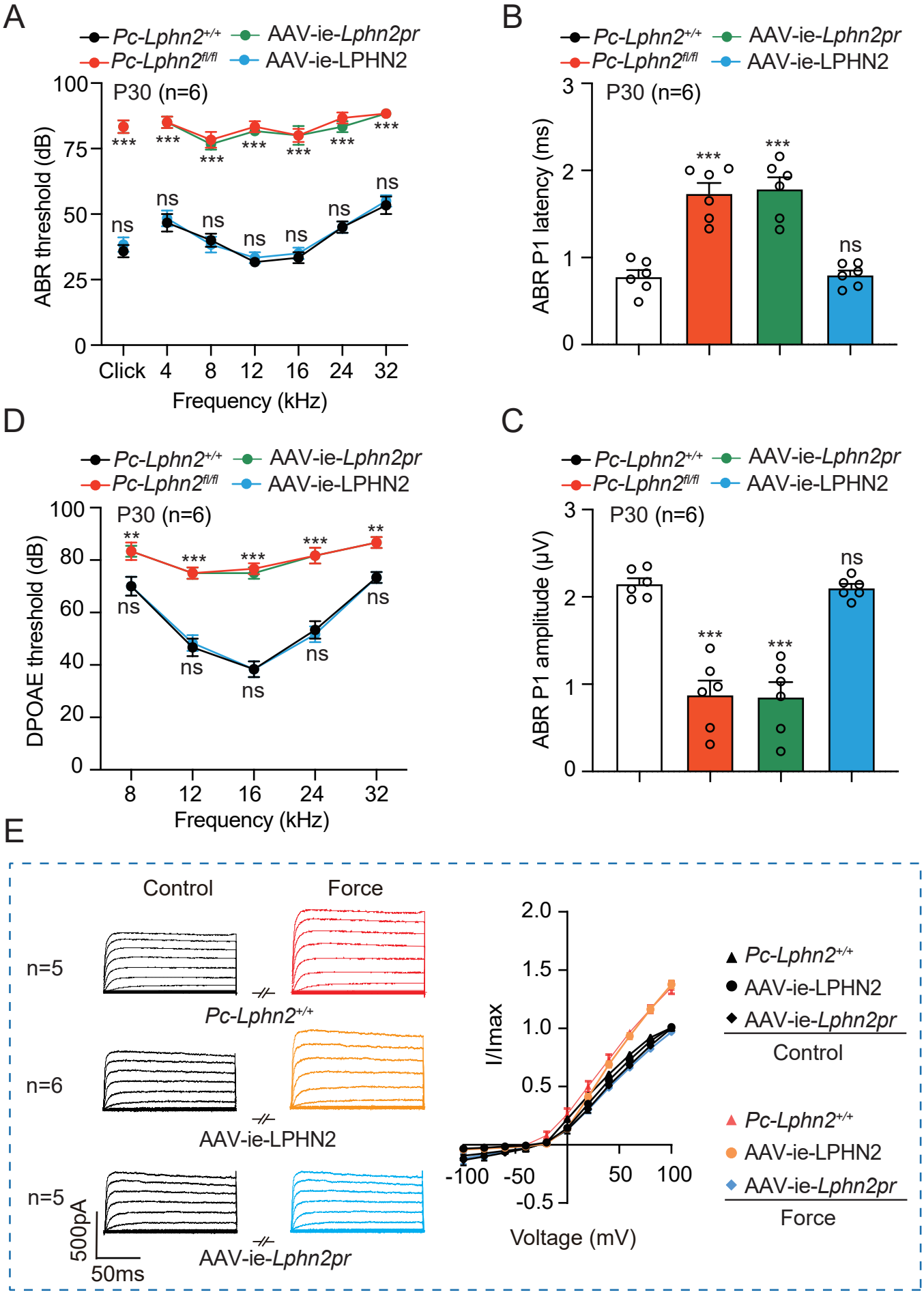
A
Pc-Lphn2+/+
Pc-Lphn2fl/fl
AAV-ie-Lphn2pr
AAV-ie-LPHN2
P30 (n=6)
ABR threshold (dB)
Frequency (kHz)
Click
4
8
12
16
24
32
B
ABR P1 latency (ms)
C
ABR P1 amplitude (μV)
D
DPOAE threshold (dB)
E
Control
Force
n=5
n=6
n=5
500pA
50ms
I/Imax
Voltage (mV)
F
21%
79%
22%
78%
100%
Force sensitive
Force insensitive